

In-operando optical observations of alkaline fuel cell electrode surfaces during harsh cycling tests

Richard Dawson^{a+}, Anant Patel^a, Kolade Alako^a, Samritha Parhar^a, Christopher Hinde^b, Christopher Reynolds^b

a. Engineering Department, Faculty of Science and Technology, Lancaster University, Lancaster, LA1 4YR, UK

b. AFC Energy Plc, Unit 71.4 Dunsfold Park, Stovolds Hill, Cranleigh, Surrey, GU6 8TB, UK

+ r.dawson@lancaster.ac.uk

+44 (0)1524 593685

D11 Engineering Building

Lancaster University

Bailrigg

Lancaster

United Kingdom

LA1 4YR

Abstract

The durability of low-cost fuel cells is one of the last technical challenges to be overcome before the widespread adoption of fuel cells can become a reality. Most research concentrates on polymer electrolyte membrane or solid oxide fuel cells in this topic with little published regarding the durability of recirculating liquid electrolyte alkaline fuel cells. In this paper we present an investigation into the durability of this fuel cell variant under harsh load cycling, air starvation and fuel starvation conditions. In the study, making use of the high ionic conductivity of the electrolyte, a novel rig design was utilised, which allowed the surfaces of the electrodes to be constantly monitored optically during the experiments. This demonstrated the good physical durability of the anode during the test protocols whilst highlighted the instability of the manganese-cobalt spinel cathode, used in this study, during the air starvation protocols. The load cycling stability of the alkaline fuel cells used was found to be good with the standard configuration giving only around a 2.7% voltage degradation at 100 mA cm^{-2} operating point over 8000 load cycles.

Keywords:

Alkaline; fuel cell; durability; in-operando; cycling; degradation

1 Introduction

Hydrogen fuel cells are efficient clean energy conversion devices poised for widespread implementation, however, when applied to most real world applications where cycling conditions are experienced high lifecycle costs remains a major obstacle to commercialisation. Alkaline fuel cells (AFC) are attractive for their greater electrical efficiencies, up to 60% in moderate conditions [1] compared to other fuel cell types. This is largely the result of excellent oxygen reduction kinetics in alkaline media compared with acidic conditions such as those in polymer electrolyte membrane fuel cells (PEMFC) [2]. Secondly, a significant advantage of AFCs is the wide range of electrocatalysts (including low cost, non-noble metal based materials) which can be used for both electrode reactions, although stability and activation issues exist [3, 4]. Another attractive feature is that concentrated alkaline electrolytes are highly ionically conductive compared to the electrolyte in other fuel cells where ultra-thin electrolytes must be used to achieve similarly low electrolyte resistive losses [5]. Despite this, alkaline fuel cells have never been produced in commercial quantities. During the latter part of the 20th century, research in alkaline fuel cells waned as interest in other types of fuel cells increased [6]; however, with recent advances in materials and processes in the intervening period, opportunities for producing commercial alkaline fuel cell systems have become apparent. This can be seen by the success of UK based alkaline fuel cell developer, AFC Energy Plc, who demonstrated their 240 kW 'KORE' system at the Air Products Stade site in Germany during early 2016.

There are two primary variants of alkaline fuel cell systems; immobilised electrolyte and re-circulating liquid electrolyte. Immobilised alkaline cells can be easier to manage due to their system simplicity; however, this variant requires very careful CO₂ management as carbonates formed by reaction of the hydroxide with carbon dioxide in the air cannot be easily removed. Carbonates act to degrade the performance of the cell through reducing the conductivity of the electrolyte [7]. The second type of alkaline fuel cell, the re-circulating liquid electrolyte cell, is able to resolve this issue by transporting the carbonate outside the cell and processing it externally. Other key benefits of recirculating AFCs are their ability to manage heat and water removal from the fuel cell reliably and accurately, as the electrolyte provides an efficient transfer medium.

The degradation rates of fuel cells in real world applications is currently the most significant direct technical barrier to the adoption of fuel cells as power sources for wide spread application.

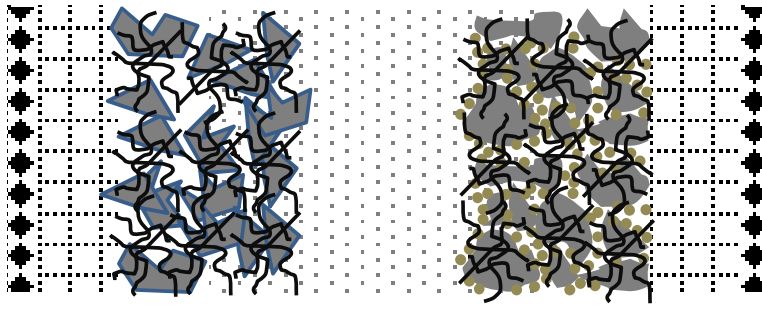
Degradation studies, materials and design innovations to improve degradation rates in two of the most studied fuel cell classes, PEMFC and SOFC, are favoured topics as can be witnessed by the amount of research published in this field but, the degradation of liquid electrolyte alkaline fuel cells

is not a well-researched topic. Most existing data is fairly limited, such as a series of post-mortem studies conducted on classical electrode designs [8, 9] or specific studies on the effect for carbonates [7]. Karl Kordesch, a prolific researcher in the field of AFC device development, published and presented many papers on the subject from the 1970s to the early 2000s. He showed that many of the degradation modes experienced by PEMFC such as electrocatalyst agglomeration, carbon corrosion and current collector corrosion could be experienced by AFCs, but some particular degradation mechanisms, such as loss of hydrophobicity by de-fluorination of PTFE and layer cracking due to high hydroxide concentrations, were also evident [10-12]. Kordesch showed reasonable cycling performance of the AFC systems being developed at University of Graz as a continuation of the Union Carbide designs [13] and authors including Tomantschger and Kordesch have shown that Pt on carbon catalysts show greater Pt agglomeration during cycles than in acid media in *ex situ* experiments [11, 14]. Again these were all based on post-mortem analysis which can be problematic. Post-mortem analysis by its very nature requires samples be extensively dried and prepared which essentially removes a significant body of the evidence – the electrolyte. Hence the research presented here aimed to develop a test rig and method where the fuel cell is “opened out” and observations made, in this case optically, to allow *in-operando* studies of degradation to be made.

The subject of accelerated tests and cycling durability has been extensively investigated for other fuel cell types whereas for AFCs there is very little knowledge in this area. Therefore, accelerated testing by load, air starvation and fuel starvation are used as a test cases to demonstrate the method whilst showing an aspect of AFC performance which has not been extensively investigated.

1.1 Alkaline fuel cell structure

The kinetics of hydrogen oxidation in alkaline media are favourable and the conditions allow the use of low cost catalysts unsuited to rival low temperature technologies. These include Ni in various forms and low %wt non-platinum precious metals supported on carbons [15, 16]. Bulk Ni based materials such as Raney Ni have been shown to have poor stability at constant running as well as activation problems [9]. The choice of cathode materials is even wider than that for the anode and can range from Pt through to spinels and perovskites usually found in SOFCs [17-19]. Silver, although a suitable material and a good oxygen reduction catalyst, requires care when used in the cathode as at open circuit potential dissolution occurs to form AgO^- [20] limiting cell life [21]. State-of-the-art cathodes are likely to be based on the ceramic materials similar to those in SOFCs although the electrode structure is different using around 75% wt or more conductive carbon fillers bound with a hydrophobising polymer (PTFE). Figure 1 shows the typical architecture of a liquid electrolyte alkaline fuel cell.



Legend


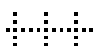





-  Liquid electrolyte (KOH)
-  Gas Diffusion Layer
-  High surface area nickel powder with passivating layer
-  Carbon black powder
-  High surface area ceramic nanopowder electrocatalyst
-  Porous metal (nickel) current collector mesh
-  Hydrophobising and binding agent (usually PTFE)

Figure 1: Standard structure of alkaline fuel cells with liquid electrolyte. Diagram shows PTFE bound layers on a gas diffusion layer with a conductive porous metallic backing.

The conditions within the cathode structure are particularly harsh; high potentials and very high local hydroxide concentrations (when at load) can lead to a number of degradation mechanisms:

1. Support corrosion – particularly when carbons are used as the conductive support material;
2. PTFE defluorination – leading to loss of hydrophobicity and breakthrough of electrolyte into gas diffusion layer;
3. Hydroxide crystallisation – dependent on air flow, humidity and the porosity and location of the triple phase boundary, hydroxide could crystallise and cause structural damage to the electrode as well as a transport limitation;
4. Carbonate formation - CO₂ in the air may cause structural damage to the electrode [10, 11, 13, 22].

The rig designed and developed by the authors presents a method by which such structural degradation can be simply observed. Results are presented for optical observations but the same principles, with modifications to the rig, would allow other imaging and spectroscopic techniques to be applied. These could capture deep structural change and other non-structural mechanism previously discussed which may also take place leading to loss in performance

2 Design of optical access rig

The alkaline fuel cell test rig developed for the purpose of structural degradation observations is shown in Figure 2.

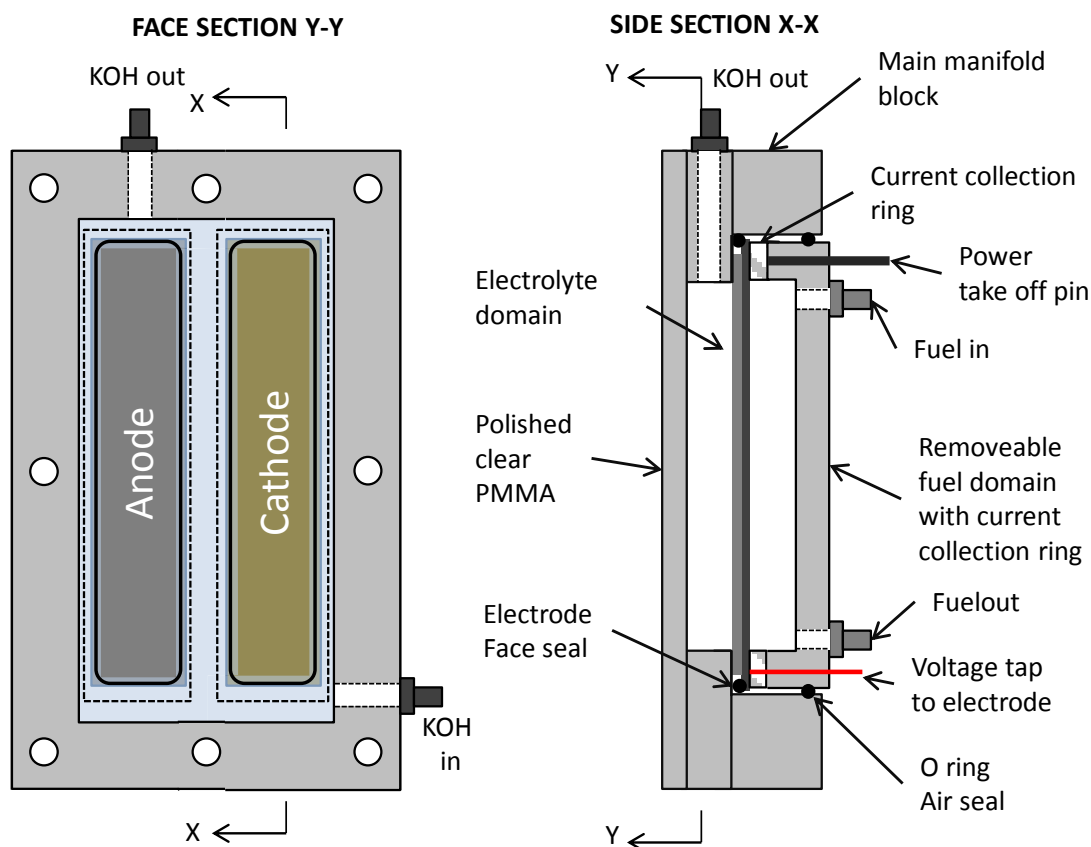


Figure 2. Fuel cell test rig schematic showing side-by-side electrode configuration giving line of sight optical access to the faces of the electrodes.

The high conductivity liquid electrolyte allows an unusual electrode configuration to be used giving line-of-sight access to the surface of each electrode during operation. Rather than face-to-face the electrodes are configured side-by-side with an electrolyte domain across the face of the electrodes. The rig materials used is Polymethyl methacrylate (PMMA) which when polished gives good transparency to visible light and is also sufficiently stable in strong hydroxide for use in alkaline fuel cell rigs. Behind the anode and cathode are simple hydrogen and air (respectively) flow domains supplying reactants and removing water as vapour. Current is collected from each electrode nickel backing by a current collector ring which also has a voltage sense connection. Hydroxide resistant seals are used to give the required electrolyte to electrode and electrode to gas domain seals. The rig is configured to allow simple removal and replacement of electrodes. The active geometric area for the electrodes were 16 cm²

3 Experimental Methods

3.1 Materials and equipment

In all experiments 30%wt KOH was used made up with ultra pure water (Elga PURELAB Flex3 with a resistivity of 18.2Mohmcm) and high purity KOH flake from ReAgent. High purity 'research' grade hydrogen (N5.5) from BOC was used for the hydrogen fuel, and filtered and CO₂ scrubbed (Sufnolime absorbent) air used for the cathode to give carbon dioxide free air.

The electrolyte flow circuit consists of a recirculation loop of 1 dm³ capacity. Electrolyte (and consequently rig) temperature was controlled by an inline heater with electrolyte pumped by a gear pump. A constant flow rate of 80 ml min⁻¹ was used for all experiments. Though initial tests were conducted at a number of temperature set points the results reported here are all for 70 °C which represents a commonly used temperature for non-pressurised systems [6] and combined with the 30%wt KOH gives close to optimum electrolyte conductivity (1.5 S cm⁻¹ [23]). The piping used is the Swagelok PFA range. All parts of the electrolyte circuit have high corrosion resistance to alkaline media. The fuel cell operation is controlled by a Scribner 890e test station incorporating a built in impedance analyser. Mass flow controllers used with the Scribner were supplied by Alicat and appropriately sized for the rig. A nitrogen purge facility is included which automatically purges the anode side should from expected norms of voltage and temperature be experienced. The rig was operated in specially design laboratory in compliance with UK DSEAR 2002 (Dangerous Substances Explosive Atmospheres) regulations. This allowed for adequate control of risks for extended unattended running.

The electrode materials as bilayer structures (gas diffusion and active layers) laminated onto a porous nickel current collector were sourced from AFC Energy Plc. Although a non-current version of the cell architecture a degree of commercial sensitivity exists regarding the exact construction. However, the anode active material was a 5%wt Pd on carbon catalyst bound with PTFE whilst the cathode active material was high surface area manganese- cobalt spinel (Mn_{1.5}Co_{1.5}O₄) blended with conductive carbon and bound with PTFE. The same materials batches and electrode construction was used in all experiments.

3.1.1 Testing protocols

Three different sets of cycling tested were defined to explore idealised load cycling of alkaline fuel cells and their response to air and fuel starvation events whilst under load. The first mimicked idealised rapid loading and unloading to accumulate a large number of cycles over a short time as an accelerated stress test similar to those specified by the US Department of Energy [24]. The second

two starvation protocols were designed to simulate extreme disturbances in the fuel and air supply to AFCs and examine how resilient they are to such events. The three protocols are summarised in Table 1 and were applied to the cell after an initial period of stabilisation at open circuit voltage.

Step	Rapid cycling protocol	Air starvation protocol	Fuel starvation protocol
1	Rapid cycling between 0 A and 0.5 A at 50 mA s^{-1} (equates to cell voltage scan of 0.8 V – 0.4 V with no recovery at open circuit) for 1000 cycles	Stabilise at -0.64 A (high power point) for 2 minutes then stop air flow	Stabilise at -0.64 A (high power point) for 2 minutes then stop fuel flow and start nitrogen purge of fuel side (0.5 slm)
2	Stabilise cell at 0.4 A output and run impedance spectra with 10% perturbation	Remove load when voltage collapses to 0.1V.	Remove load when voltage collapses to 0.1V.
3	Repeat steps 1 and 2 till cell deemed to fail (0.1 V)	Restart air flow and stabilise cell at open circuit for 2 minutes	Restart fuel flow (stop nitrogen flow) and stabilise cell at open circuit for 2 minutes
4		Run rapid cycled current scan from 0 A to 0.8 A at 50 mA s^{-1}	Run rapid cycled current scan from 0 A to 0.8 A at 50 mA s^{-1}
5		Stabilise cell at 0.64 A output and run impedance spectra with 10% perturbation	Stabilise cell at 0.64 A output and run impedance spectra with 10% perturbation
6		Repeat steps 1 to 5 till cell deemed to fail	Repeat steps 1 to 5 till cell deemed to fail

Table 1: Details of testing protocols used in the optical access experiments

When using the optical access rig distinguishable features on the electrode were located and marked in the images in the IMetrum video gauging software for location tracking. In the case of the rapid cycling test, points on both anode and cathode were tracked (though this negated the use of 3D, which required two cameras to give a stereo image, due to field of view limitations) whereas for the air and fuel starvations tests only the cathode and anode respectively were tracked (in 3D). Due to the lack of contrast in the surfaces it was difficult to track homogenous parts of the layers, so small variation in binder and small defects were tracked. It had initially been intended to run the cycling

test at the same current points as the starvation tests but an anode delamination from the current collector backing, which was not visible at assemble (but became worse during testing and was subsequently visible on disassembly) limited the performance of this cell and consequently the current points had to be reduced.

For the fuel starved cell a final more aggressive cycle was applied where the cell was drawn down to 0.1 V for 2 minutes heavily polarising the fuel cell, particularly the cathode, the fuel supply was then set to zero (fuel side purged with nitrogen as previously) and the cell continued to be run at 0.1 V for a further 10 minutes. After this the fuel was restarted, the cell allowed to regain an open circuit potential and its impedance analysed though at a current point of 0.2 A to allow for the effect of the rapid degradation. Impedance analysis at this current point showed no difference to the last measurement made at 0.64 A in the previous protocol.

As a baseline for comparison with a more conventional rig design a version of the rapid cycling protocol was conducted. In this rig square coupons of the same electrode materials were used which had an active area of 11.8 cm^2 . The same flow rates of electrolyte, fuel and air were used along with the same temperature set point. However, the electrodes were conventionally facing each other with a uniform electrode gap of approximately 3 mm which was over an order of magnitude shorter than that in the optical access rig.

4 Results and Discussion

4.1 Standard configuration baseline cycling durability

Figure 3 shows the results of rapid cycling on the conventional configuration cell. Initial appearances from the polarisation curves suggest that there is very little change in performance. At a current density operating point of 100 mA cm^{-2} the voltage degradation from the maximum achieved is only around 2.7% after 8000 cycles (approximately 43 hours of testing). On closer examination of the impedance spectra in Figure 3B it can be seen that at least two things are changing in the performance of the cell. Firstly the series connected resistance is reducing and secondly the polarisation resistance of one of the electrodes are increasing. The electrolyte concentration and temperature are steady and so are an unlikely source of the any reduction in series resistance, however, the most likely course is the progressive wetting of the active region of the electrodes during the initial operation. This leads to a reduction in the electronic conduction path length to the current collector and so a slight improvement in series resistance. The increase in charge transfer resistance could be either attributed to instabilities, both physical and chemical, of the Pd anode and ceramic cathode catalysts.

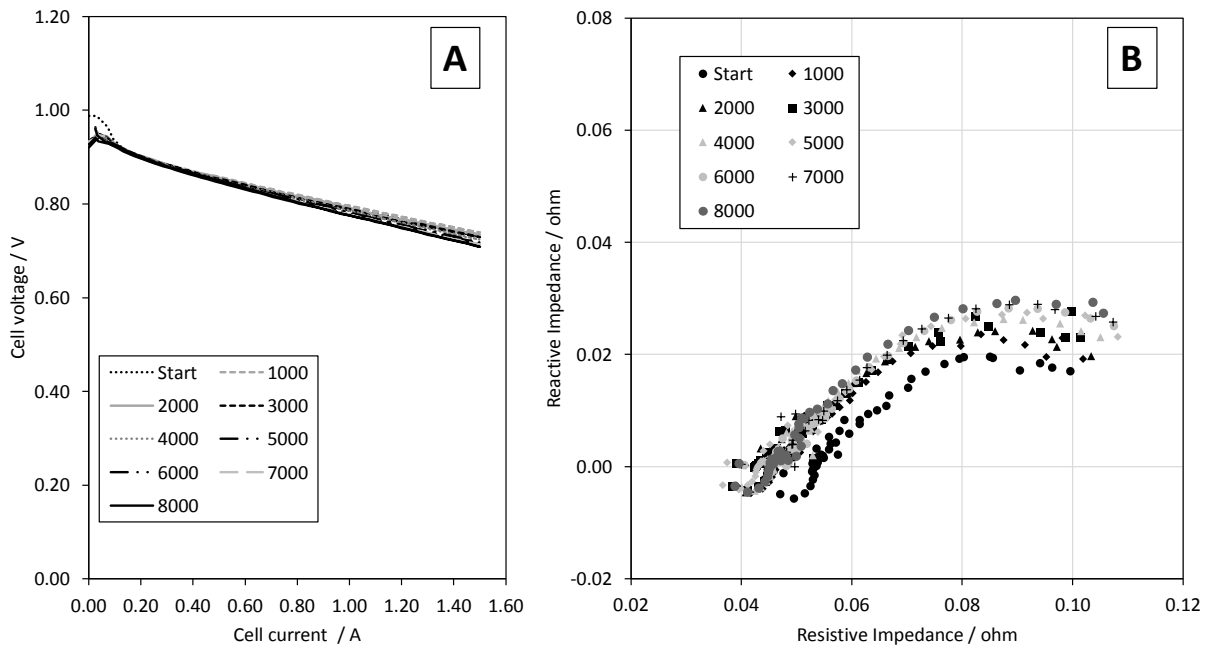


Figure 3. Baseline rapid cycling test results conducted for 8000 cycles on electrodes with active area 11.8 cm^2 at $70 \text{ }^\circ\text{C}$, 0.5 slm air and 0.2 slm hydrogen. A: current voltage response scanned at 5 mA s^{-1} 0 to 1.5 to 0 A. B: Impedance response at 0.8 A and 10% perturbation in current between 10 kHz and 0.1 Hz.

It is possible to use a basic equivalent circuit model to give an indication of the how the electrodes are changing during cycling. A simple circuit proposed is given in Figure 4. At the current point chosen for the EIS measurements it can be seen that the series resistance improves by around 13% whilst the electrode resistances (dominated by charge transfer rather than mass transfer) increase by around 17% giving a slight degradation overall in performance. Over 8000 cycles the degradation rate equates to 3 mV per 1000 cycles at a current density of 100 mA cm^{-2} . The current density is more modest than the usual for PEMFC targets [25] but it still demonstrates that AFCs are durable to load cycling in idealised accelerated stress tests.

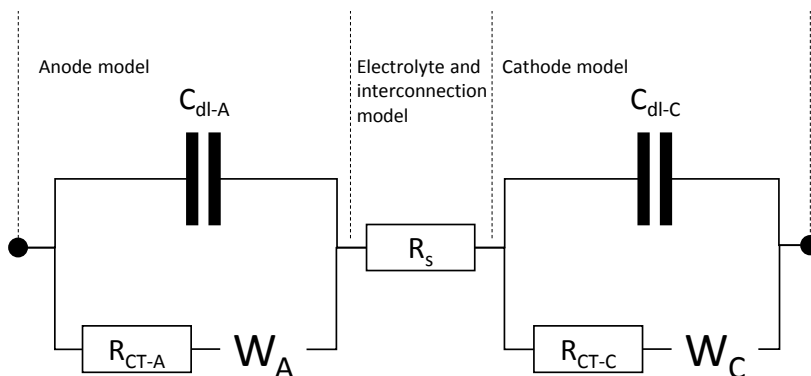


Figure 4: Simple electrode model for a fuel cell. R_{CT} – Charge transfer resistance, W – Warburg element C_{dl} – double layer capacitance

4.2 Optical access results

The rapid cycling protocol optical access results are shown in Figure 5 and Figure 6. There are some notable differences in the performance of the cell in this experiment compared to the more standard set up.

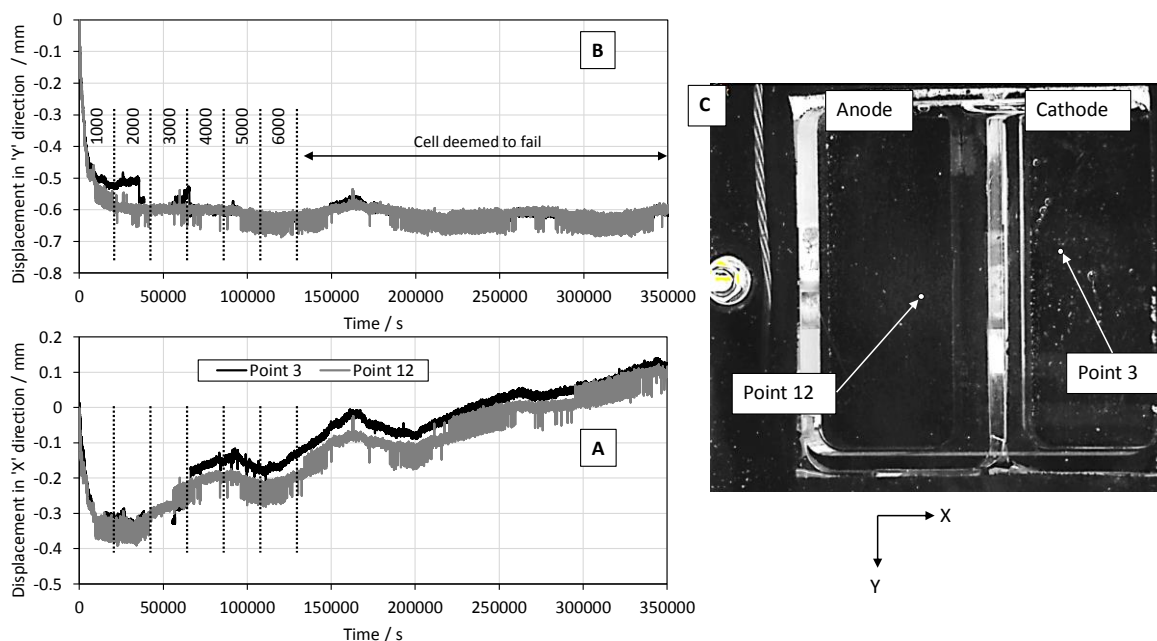


Figure 5: Optical access X and Y displacement results for two example points for load cycling protocol. Point 3 on cathode and point 12 on anode. Number of cycles are marked. A: X displacements, B: Y displacements, C: image of rig with points marked.

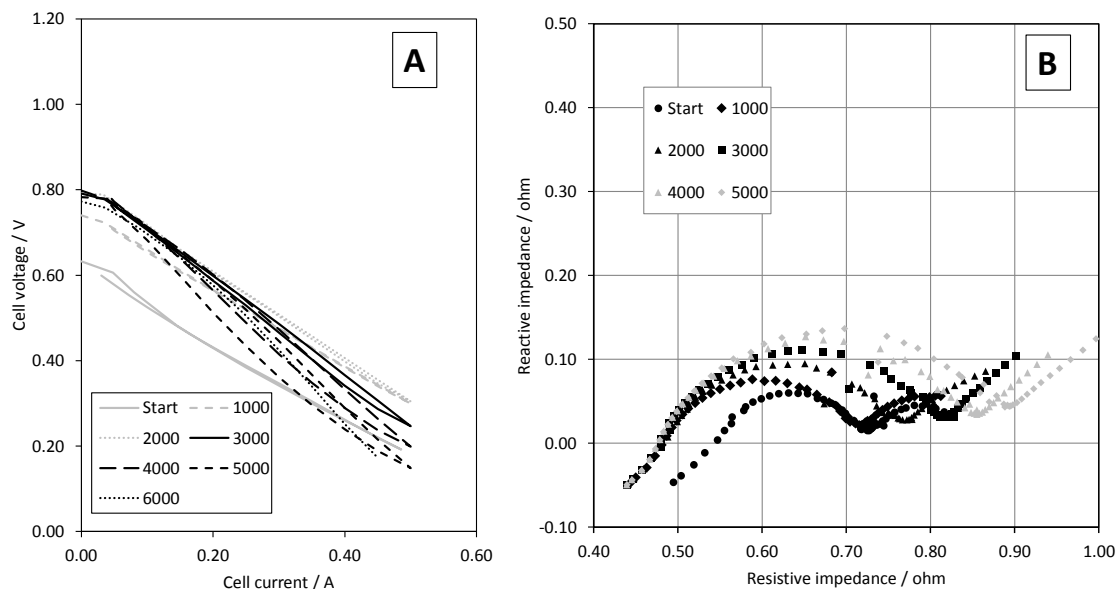


Figure 6: Load cycling results for 6000 load cycles on optical access rig set up, on electrodes with active area 16 cm^2 at $70 \text{ }^\circ\text{C}$, 0.5 slm air and 0.2 slm hydrogen. Cell temperature set point; $70 \text{ }^\circ\text{C}$, electrolyte concentration; $30\% \text{ wt KOH}$. A: polarisation, 0 to 0.5 to 0 A at 50 mA s^{-1} B: Impedance Nyquist plot for 0.4 A with 10% perturbation from 10 kHz to 0.1 Hz .

In Figure 5 it is clear to see that the series resistance of the optical access rig is around 10 times greater. This is in keeping with the increased electrolyte current path though this in practice is complex due to the side by side configuration. The same percentage reduction in series resistance is experienced (13%) during running as for the face to face configuration and can be explained again by the electrodes wetting with electrolyte and the triple phase reaction boundary becoming defined deeper within the electrode. This is observed in the optical results particularly for the cathode where bubbling can be witnessed in Figure 5D at the start of the experience but not in Figure 5E at the end.

The cell failed (voltage dipped below 0.1 V) at around 6000 cycles whereas the face to face configuration was only slightly degraded at 8000 cycles. Figure 6 gives some indications as to the reasons for failure. The polarisation curves in Figure 6A show a rapid degradation and hysteresis in the curves indicating an increased diffusion resistance in the electrodes. This is further emphasised in the impedance spectra of Figure 6B which now displays significant transport resistance. It should be noted that although the current point of 0.4 A gives much higher apparent cell polarisation than for the face to face rig around 200 mV of this is due to resistive loss in the electrolyte such that the polarisation of the electrodes is much more modest than initially appears. Using the simple model given in Figure 4 and by making the assumption that anode charge transfer and mass transfer resistances are smaller than those of the cathode, a simple estimation of the component values were made using an impedance analysis software linked with the fuel cell test station (ZView, Scribner Associates). The charge transfer and mass transfer resistances combined for the anode and cathodes in all the tests at the start and end are shown in Figure 7 which suggests that the largest deterioration in performance could be attributed to the cathode. These resistances and deteriorations are much greater than for the face to face rig. This can be attributed in part to the lower voltage operating point (even considering pure series resistive loss difference) but is likely largely attributable to the transport resistance being much larger than in the face to face. Both the gas and electrolyte flow in the optical access rig are much less uniform and idealised than in the face to face rig. This likely led to fouling by water in the gas diffusion layers possibly giving breakthrough of electrolyte into the gas diffusion layer and rapid irreversible loss of performance.

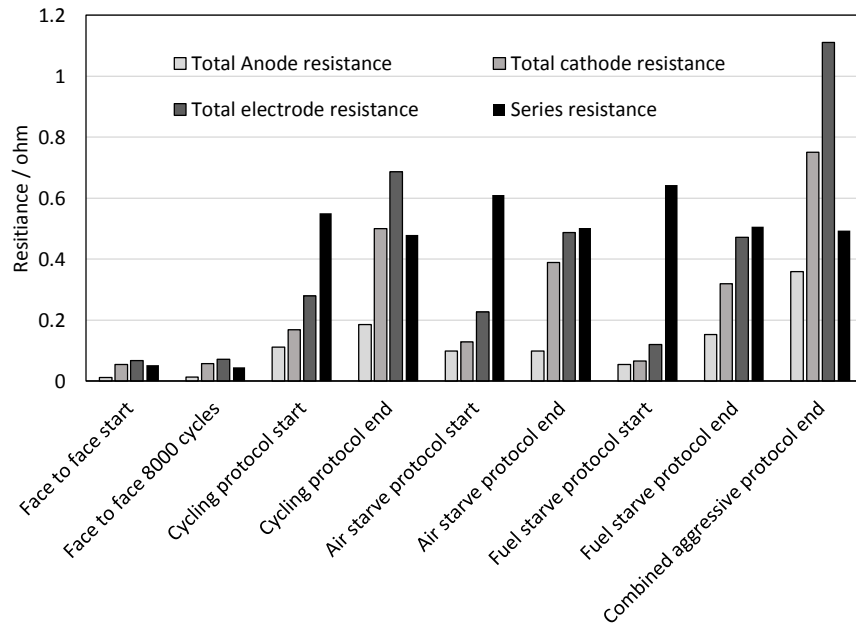


Figure 7: Summary of approximate electrode resistance from basic fitting of simple equivalent circuit of Figure 4. Approximate resistances (both charge transfer and mass transfer) for each electrode are given, the total electrode resistance and the series resistance (electrolyte and interconnection) for each cell at the start and end of the protocols conducted.

The displacement measurements shown in Figure 5 don't give further information on the degradation mode experienced in cycling but confirm that wetting of the cathode in preventing air crossover is important and that both electrodes at the active layer remain intact without any visible material loss or change. Elemental analysis by EDAX (Jeol EX-94400T4L11 with ultra-thin film window suitable for Be to U) post-mortem compared to fresh material gives further information on change produced by the test. This is given for the anodes and cathodes of all tests in

Table 2. The fluorine content which is associated with PTFE is the most stable constituent of the electrodes and is well interconnected. This means any relative increase in fluorine percentage suggests a loss of other components from the surface. Considering the anode the changes appear insignificant though the slight apparent reduction in Pd content may be an artefact of changing Pd distribution and loss of surface area. Considering the cathode the change in the composition again is minor supporting the observations of no significant surface changes to the electrode. The changes that do occur are mostly attributable to slight dissolution of the Co from the spinel and oxidation of the carbon leading to oxygen containing groups on the carbon surface.

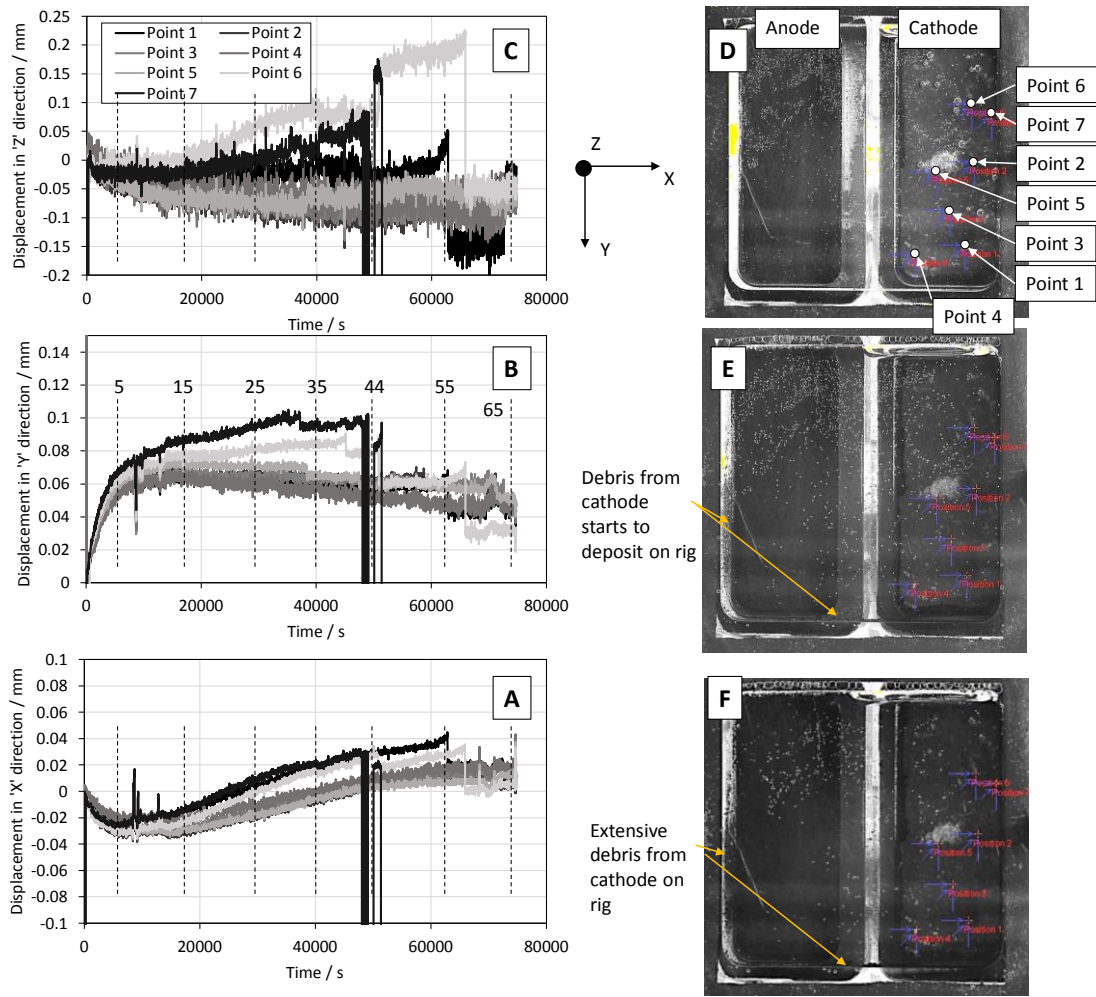


Figure 8: Optical access X, Y and Z displacement results for seven example points on the cathode for the air starvation protocol. Number of cycles are marked. A: X displacements, B: Y displacements, C: Z displacements, D: image of the rig at the start with monitoring points highlighted, E: image of the rig after 10 hours showing the start of observable debris in the rig, F image of the rig as the end showing significant debris in the rig.

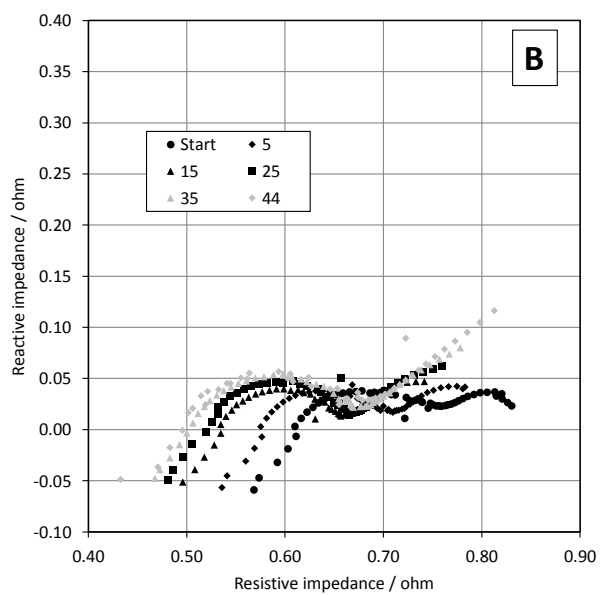
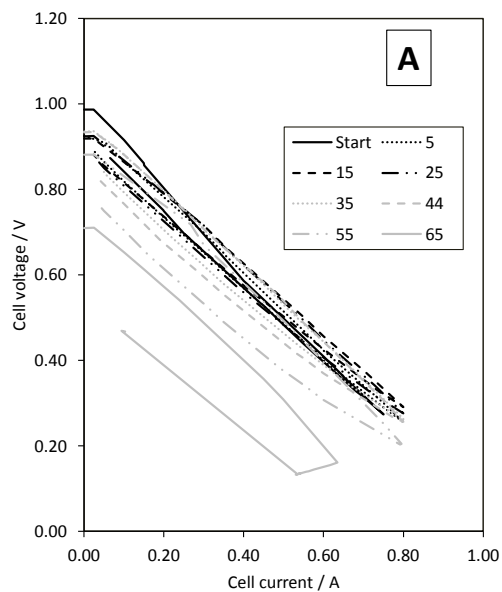


Figure 9: Air starvation results for 65 cycles on optical access rig set up on electrodes with active area 16 cm^2 at $70\text{ }^\circ\text{C}$, 0.2 slm hydrogen and air cycled between 0 and 0.5 slm . A: polarisation, 0 to 0.8 to 0 A at 50 mA s^{-1} B: Impedance Nyquist plot for 0.64 A with 10% perturbation from 10 kHz to 0.1 Hz .

The air starvation protocol had a much more significant effect on the cell. The results can be seen in Figure 8 and Figure 9. The starting performance of these electrodes were significantly better than other used in the cycling protocol and had no substrate to current collector delamination observed post-test on disassembly. Increasing cathode contribution to the impedance is particularly apparent as shown in Figure 7 and Figure 9B. The cathode degradation produces very visible debris in the rig (Figure 8E and F) and in the displacement traces (Figure 8A, B and C) start to coincide with detectable events at the monitoring points. These become more frequent and significant as the test progresses and very much more significant beyond 44 cycles which was the point at which the EIS current point could no longer be sustained and the performance of the cell in the polarisation curves (Figure 9A) began to degrade more rapidly. The EDAX composition data (

Table 2) shows that again the anode changes slightly but during this test the cathode composition has been significantly altered. The data shows that the active catalyst has been lost with a selective leaching of the cobalt. The manganese : cobalt ratio has reduced from $1:1$ to $1:0.61$ and as a major component of the electrode has led to the physical erosion. This is supported by the increased percentage of fluorine in the surface. The loss of cobalt from the spinel can be explained by examining the relative stabilities of the simple oxides of both manganese and cobalt. In the pH 14.7 polarising the cathode by around 700 mV would start to lead to the formation of the HMnO_4^- ion [20] whereas a polarisation of only 100 mV would allow the formation of the HCoO_2^- ion to begin [20]. This gives no indication of the kinetics but in the harsh test in the air starvation protocol where the cell voltage is allowed to drop to 0.1 V there will be significant driving force for the cobalt reduction and dissolution to occur as observed. Away from the electrode and with the dissolved oxygen content in the electrolyte this species is likely to be reoxidised and precipitate out as the simple oxide adding further to the debris observed.

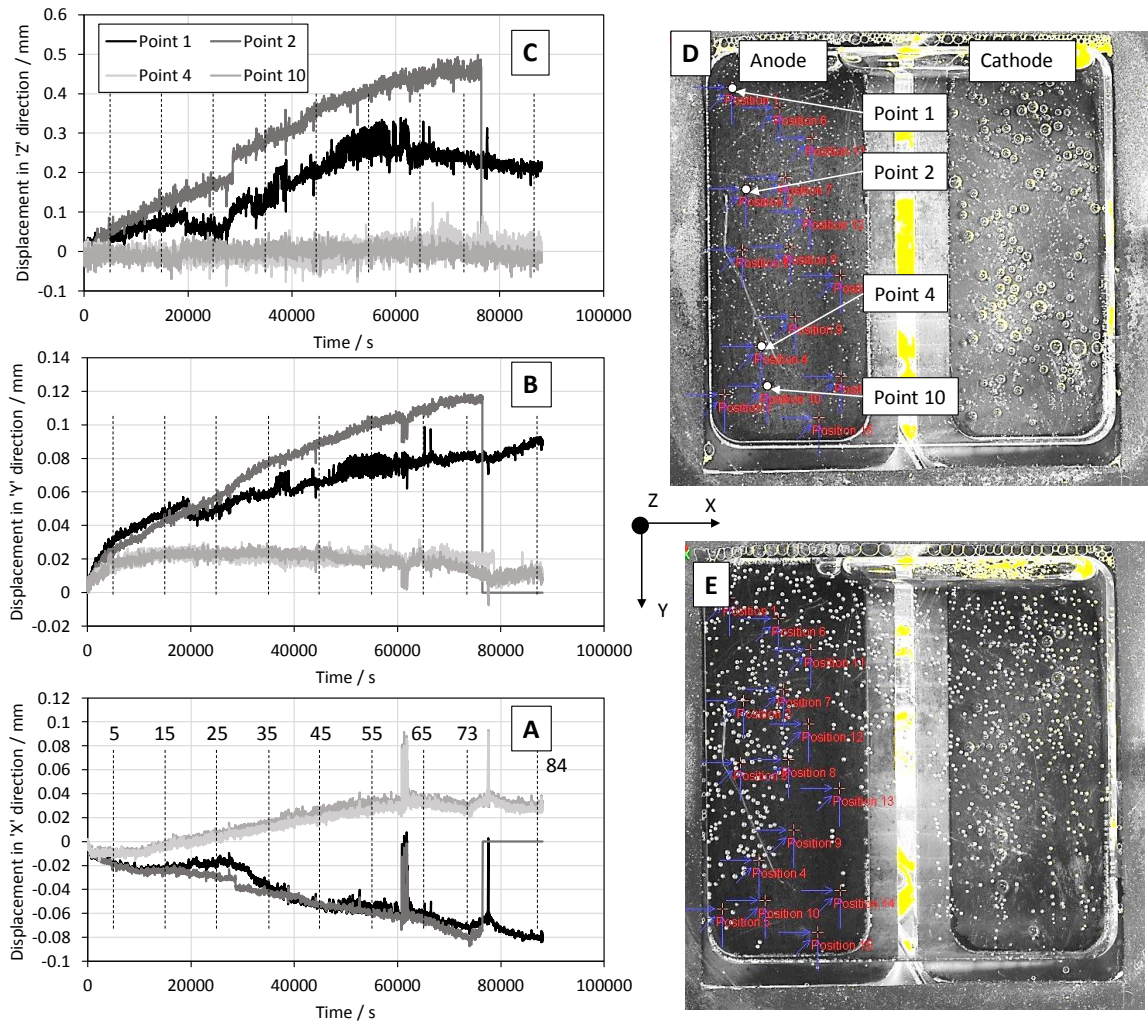


Figure 10: Optical access X, Y and Z displacement results for four example points on the anode for the fuel starvation protocol. Number of cycles are marked. A: X displacements, B: Y displacements, C: Z displacements, D: image of the rig at the start with monitoring points highlighted, E image of the rig as the end of 84 cycles.

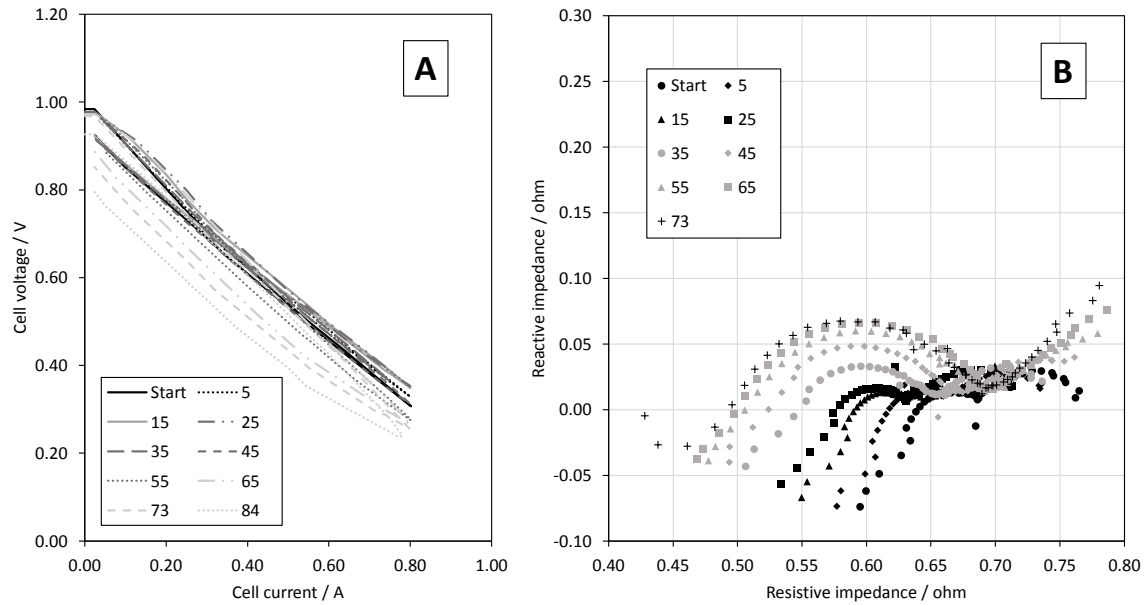


Figure 11: Fuel starvation results for 84 cycles on optical access rig set up on electrodes with active area 16 cm^2 at $70 \text{ }^\circ\text{C}$, 0.5 slm air and hydrogen cycled between 0 and 0.2 slm alternately with nitrogen at 0.5 slm . A: polarisation, 0 to 0.8 to 0 A at 50 mA s^{-1} B: Impedance Nyquist plot for 0.64 A with 10% perturbation from 10 kHz to 0.1 Hz .

The fuel starvation protocol had a more significant effect on the performance of the anode as would be expected and can be seen in Figure 7 and Figure 11, however, in all tests with the optical access rig there is an apparent degradation in transport which is not seen in the face to face rig. This is in both electrodes but more pronounced for the cathode as would be expected given diffusion limitations of 21% oxygen in air. This is a rig specific effect and highlights the importance of good air and hydrogen flow field design in alkaline fuel cells. More difficulty was experienced when tracking the points in the rig for this test than previously as electrolyte degassing caused bubble formation on the inside surface of the rig window obscuring the view of the electrode. It was later noted that the electrolyte in this test had been allowed to cool after being generated from flake allowing gas to redissolve in the electrolyte and later give the degassing problem on reheating in the rig. Hence only 4 points were successfully tracked. Excluding point 4 (see Figure 10) little evidence is present of significant events equivalent to the structural degradation of the cathode in the air starvation protocol. This is supported by the lack of observable debris in the rig and flow circuit.

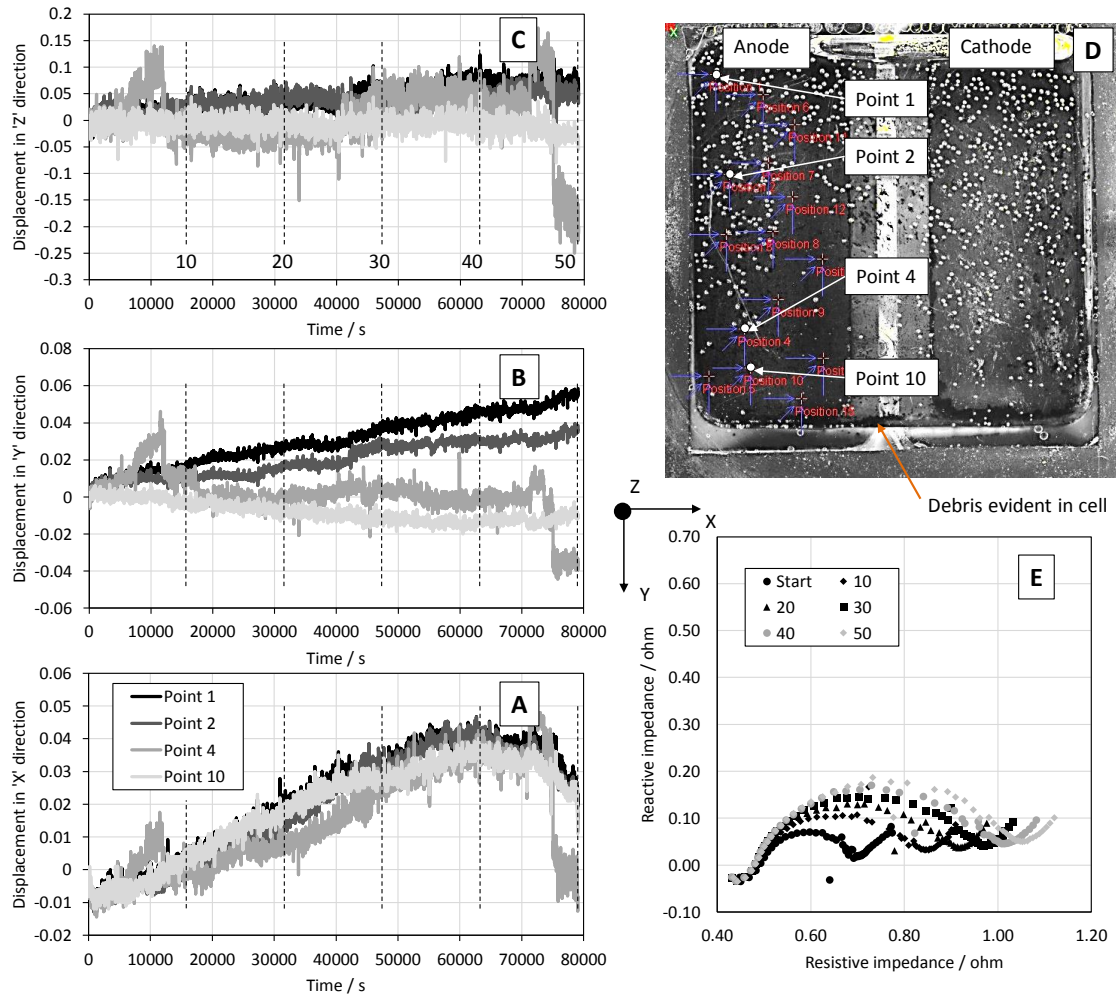


Figure 12: Aggressive cycling results for 50 cycles on optical access rig set up on electrodes with active area 16 cm^2 at $70 \text{ }^\circ\text{C}$, 0.5 slm air and hydrogen cycled between 0 and 0.2 slm alternately with nitrogen at 0.5 slm . A: X displacements, B: Y displacements, C: Z displacements, D: image of the rig at the end with monitoring points highlighted and significant evidence of debris from cathode, E Impedance Nyquist plot for 0.2 A with 10% perturbation from 10 kHz to 0.1 Hz .

The fuel starvation cycle continued straight into the final combined anode and cathode aggressive cycling test which repeatedly heavily polarised first the cathode then the anode. The equivalent results are shown in Figure 12. Again tracking the points on the anode surface show little sign of physical degradation of the anode. However, Figure 12D clearly shows debris from the cathode has been generated again by the high cathode polarisation during the cycle. The cell impedance spectra Figure 12E and basic model fitting (Figure 7) suggest steady degradation in performance of both electrodes but again proportionally more attributable to the cathode. The EDAX measurements made on these electrodes after the two protocols confirms that the anode does not suffer structural or compositional degradation even in these harsh cycle conditions, though catalyst agglomeration is likely and a steady increase in transport resistance related to the rig design is observed. The cathode composition shows very clearly an extreme degradation of the layer where the manganese : cobalt

ratio is now 1:0.57 and the increase in the proportion of fluorine and hence the overall loss of the bound powders is significant.

Element / ratio	Cycling	Air	Fuel	Fresh
Cathode compositions (%weight)				
C	0.79	0.83	0.79	0.75
F	0.16	0.13	0.17	0.18
Pd	0.05	0.04	0.04	0.07
Anode compositions (%weight)				
C	0.28	0.28	0.33	0.22
O	0.20	0.18	0.10	0.15
F	0.09	0.15	0.33	0.08
Mn	0.21	0.23	0.15	0.28
Co	0.22	0.15	0.09	0.27
Spinel atomic ratio in cathode (Mn:Co)				
1:Co	0.96	0.61	0.57	1.10

Table 2: EDAX electrode composition (surface) results for fresh electrodes and those used in the optical access experiments.

5 Conclusion

An optical access rig for liquid electrode alkaline fuel cells has been successfully developed to monitor the surface of fuel cell electrodes during operation. Changes in electrodes have been observed during load cycling, air starvation and fuel starvation protocols. The active cathode (catalyst constituent was $Mn_{1.5}Co_{1.5}O_4$) was severely damaged by air starvation and cycling which brought the cathode potential down to a potential region where the Co component could rapidly reduce and form a soluble complex. This was observed by changes in impedance and witnessed by physical erosion events on the electrode surface resulting in a build-up of debris in the rig and flow circuit. The change in composition and loss of components was confirmed by EDAX measurements. Physically the active anode layer was much more durable than the cathode with no observable erosion events during starvation cycles, however, the cycles did result in a drop in performance most likely attributable to agglomeration of the Pd catalyst. The rig design did allow for simple observation of the electrodes surfaces by an IMetrum 3D optical gauging system but the flow fields within the design were not as optimal as the standard face to face rig. This could be seen by a steadily increasing transport resistance in both electrodes in the optical rig which was not experienced in the standard rig. This resulted in the test from the standard rig showing very little degradation in 8000 load cycles whilst the optical rig gave very significant degradation in only 6000 cycles. Overall the optical access rig has demonstrated the successful observation of electrodes and

highlighted the bulk physical stability of the anode used and the lack of chemical stability of the manganese – cobalt spinel in adverse cathode operating conditions.

6 Acknowledgments

We would like to thank Dr. Richard Wilbraham for the EDAX analysis of the electrodes, AFC Energy Plc for their provision of electrode materials.

7 Data access management

Due to confidentiality agreements with research collaborators, supporting data can only be made available to bona fide researchers subject to a non-disclosure agreement. Details of the data and how to request access are available at Lancaster University research portal: [DOI on publication](#).

8 References

1. Bidault, F., Brett, D.J.L., Middleton, P.H., and Brandon, N.P., Review of gas diffusion cathodes for alkaline fuel cells. *J.Power Sources*, 2009. 187(1): p. 39-48.
2. Li, X., Liu, G., and Popov, B.N., Activity and stability of non-precious metal catalysts for oxygen reduction in acid and alkaline electrolytes. *J.Power Sources*, 2010. 195(19): p. 6373-6378.
3. Kiros, Y. and Schwartz, S., Long-term hydrogen oxidation catalysts in alkaline fuel cells. *J.Power Sources*, 2000. 87(1–2): p. 101-105.
4. Wagner, N., Schulze, M., and Gülzow, E., Long term investigations of silver cathodes for alkaline fuel cells. *J.Power Sources*, 2004. 127(1–2): p. 264-272.
5. Gilliam, R.J., Graydon, J.W., Kirk, D.W., and Thorpe, S.J., A review of specific conductivities of potassium hydroxide solutions for various concentrations and temperatures. *Int. J. Hydrogen Energ.*, 2007. 32(3): p. 359-364.
6. McLean, G.F., Niet, T., Prince-Richard, S., and Djilali, N., An assessment of alkaline fuel cell technology. *Int. J. Hydrogen Energ.*, 2002. 27(5): p. 507-526.
7. Naughton, M.S., Brushett, F.R., and Kenis, P.J.A., Carbonate resilience of flowing electrolyte-based alkaline fuel cells. *J.Power Sources*, 2011. 196(4): p. 1762-1768.
8. Gülzow, E. and Schulze, M., Long-term operation of AFC electrodes with CO₂ containing gases. *J. Power Sources*, 2004. 127(1–2): p. 243-251.
9. Gülzow, E., Schulze, M., and Steinhilber, G., Investigation of the degradation of different nickel anode types for alkaline fuel cells (AFCs). *J. Power Sources*, 2002. 106(1–2): p. 126-135.
10. Tomantschger, K. and Kordesch, K.V., Structural-analysis of alkaline fuel-cell electrodes and electrode materials. *Journal of Power Sources*, 1989. 25(3): p. 195-214.
11. Tomantschger, K., Findlay, R., Hanson, M., Kordesch, K., et al., Degradation modes of alkaline fuel-cells and their components. *Journal of Power Sources*, 1992. 39(1): p. 21-41.
12. Cifrain, M. and Kordesch, K.V., Advances, aging mechanism and lifetime in AFCs with circulating electrolytes. *Journal of Power Sources*, 2004. 127(1-2): p. 234-242.
13. Kordesch, K., Gsellmann, J., Cifrain, M., Voss, S., et al., Intermittent use of a low-cost alkaline fuel cell-hybrid system for electric vehicles. *Journal of Power Sources*, 1999. 80(1-2): p. 190-197.
14. Zadick, A., Dubau, L., Sergent, N., Berthome, G., et al., Huge Instability of Pt/C Catalysts in Alkaline Medium. *Acs Catalysis*, 2015. 5(8): p. 4819-4824.

15. Alesker, M., Page, M., Shviro, M., Paska, Y., et al., Palladium/nickel bifunctional electrocatalyst for hydrogen oxidation reaction in alkaline membrane fuel cell. *Journal of Power Sources*, 2016. 304: p. 332-339.
16. Al-Saleh, M.A., Gultekin, S., Al-Zakri, A.S., and Khan, A.A.A., Steady state performance of copper impregnated Ni/PTFE gas diffusion electrode in alkaline fuel cell. *International Journal of Hydrogen Energy*, 1996. 21(8): p. 657-661.
17. Bo, X.J., Zhang, Y.F., Li, M.A., Nsabimana, A., et al., NiCo₂O₄ spinel/ordered mesoporous carbons as noble-metal free electrocatalysts for oxygen reduction reaction and the influence of structure of catalyst support on the electrochemical activity of NiCo₂O₄. *Journal of Power Sources*, 2015. 288: p. 1-8.
18. Ge, X., Sumboja, A., Wu, D., An, T., et al., Oxygen Reduction in Alkaline Media: From Mechanisms to Recent Advances of Catalysts. *ACS Catalysis*, 2015. 5(8): p. 4643-4667.
19. Lu, F., Sui, J., Su, J., Jin, C., et al., Hollow spherical La_{0.8}Sr_{0.2}Mn_{0.3} perovskite oxide with enhanced catalytic activities for the oxygen reduction reaction. *Journal of Power Sources*, 2014. 271: p. 55-59.
20. Pourbaix, M., *Atlas of Electrochemical Equilibria in Aqueous Solutions*. 2nd Edition ed. 1974, National Association of Corrosion.
21. Wagner, N., Schulze, M., and Güllow, E., Long term investigations of silver cathodes for alkaline fuel cells. *J. Power Sources*, 2004. 127(1-2): p. 264-272.
22. Tomantschger, K., Gsellmann, J., Kordesch, K., and Hanson, M., Operating characteristics of fuel-cell electrodes in alkaline electrolyte. *Journal of the Electrochemical Society*, 1987. 134(3): p. C129-C129.
23. Gilliam, R.J., Graydon, J.W., Kirk, D.W., and Thorpe, S.J., A review of specific conductivities of potassium hydroxide solutions for various concentrations and temperatures. *International Journal of Hydrogen Energy*, 2007. 32(3): p. 359-364.
24. DoE cell component accelerated stress test protocols for PEM fuel cells. 2007, US Department of Energy.
25. Fuel cell technologies office multi-year research, development, and demonstration plan. 2016, US Department of Energy.